Anomalous photoinduced band renormalization in correlated materials: The case of Ta₂NiSe₅

Lei Geng ®,[1] Xiulan Liu,[1] Jianing Zhang ®,[1] Denis Golež ®,[2,3,*] and Liang-You Peng[1,4,5,6,†]

[1]*State Key Laboratory for Mesoscopic Physics and Frontiers Science Center for Nano-Optoelectronics, School of Physics,*
Peking University, Beijing 100871, China
[2]*Jozef Stefan Institute, Jamova 39, SI-1000 Ljubljana, Slovenia*
[3]*Faculty of Mathematics and Physics, University of Ljubljana, Jadranska 19, SI-1000 Ljubljana, Slovenia*
[4]*Collaborative Innovation Center of Quantum Matter, Beijing 100871, China*
[5]*Collaborative Innovation Center of Extreme Optics, Shanxi University, Taiyuan 030006, China*
[6]*Beijing Academy of Quantum Information Sciences, Beijing 100193, China*

We investigate the anomalous photoinduced band renormalization in correlated materials, exemplified by the case of Ta₂NiSe₅. The manifestation of this anomaly is characterized by the alternating direction of band shift in response to changes in the laser parameters or electron momentum. We attribute the phenomena to the band inversion of the material and the selective excitation of a high-lying flat band, leading to the competition between the Hartree shift and the order collapse. These findings are based on an *ab initio* determined effective model for Ta₂NiSe₅, in which we incorporate high-lying states and the time-dependent *GW* simulation to follow the nonequilibrium dynamics induced by the laser. Our findings reveal the sensitivity of the nonequilibrium electronic dynamics to the band structure and laser protocols, providing valuable guidance for the selection of suitable materials and lasers in the engineering of band structures.

I. INTRODUCTION

The development of laser sources has provided an unprecedented opportunity to manipulate the properties of solid-state materials by strong light pulses [1–4]. Ultrafast lasers can induce long-lived nonequilibrium states in quantum materials, showcasing distinctive features not observed in their equilibrium counterparts. Recent experiments have demonstrated the potential of photoinduced nonequilibrium states in modifying ferromagnetism [5], superconductivity [6–8], or charge-density waves [9–12]. As a material's properties are closely related to its electronic band structure, it is important to understand how it can be efficiently manipulated. The understanding is further strengthen by remarkable development of time- and angle-resolved photoemission spectroscopy (ARPES), which provides a direct insight into the light-induced band-gap renormalization [13–23].

The excitonic insulator (EI) is one of the most elusive states of matter. Despite its conceptual proposal decades ago [24–26] and the implementation in artificial systems [27–29], providing conclusive evidence for its presence in real materials remains a significant challenge. The two most extensively studied candidates for the EI are 1T-TiSe₂ [30–32] and Ta₂NiSe₅ (TNS) [33–41]. For TNS, ARPES results indeed showed the presence of the flat valence-band top below a certain temperature, indicative of an ordered phase. Its origin has recently been highly debated. Valuable insights were given by time-resolved ARPES after high-frequency excitations. The most important observation is the transient downward shift of the valence band, primarily localized near the Γ point, distinguishing the response from the typical band renormalization in semiconductors [17,21,42–44]. In addition, this phenomenon is observed only above a certain pump intensity [17]. However, other experiments utilizing a different pump laser frequency reported a monotonic upward shift of the valence band [45]. These diverse results show that the direction of band shift in TNS is dependent not only on the electron momentum but also on laser intensities and frequencies, which provide compelling examples for the study of the anomalous band renormalization.

In this work, we combine the *ab initio* determined band structure of TNS [46] with the self-consistent time-dependent *GW* approximation at finite temperature [43,47–50] to study the equilibrium and nonequilibrium properties of TNS. Our results can consistently reproduce multiple phenomena observed in experiments. The underlying causes of the anomalous band renormalization are analyzed. A set of higher-lying flat orbitals not only play a role in symmetry breaking for equilibrium, but they are also responsible for a long-lived nonthermal state under a resonant excitation with respect to the valence band. The nonthermal population of the flat band significantly influences the competition between the Hartree shift and the order collapse, which can lead either to the downward or upward band shift depending on the pump protocol. The momentum dependence of the band renormalization is attributed to the band inversion of TNS. The investigation into anomalous band renormalization in TNS also provides insights for nonequilibrium processes in other materials.

*Contact author: denis.golez@ijs.si
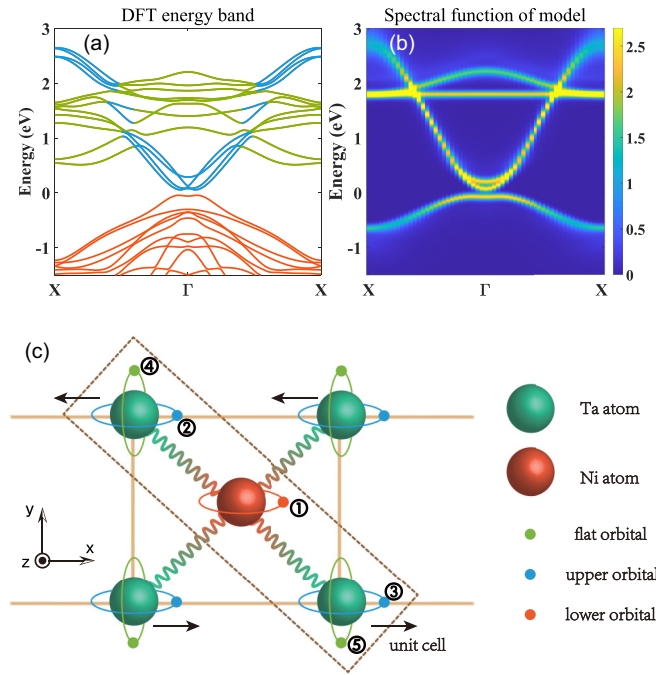†Contact author: liangyou.peng@pku.edu.cn

FIG. 1. (a) The energy bands of the TNS in the excitonic phase from the DFT calculation. The bands in orange, blue, and green represent the lower, upper, and flat bands, respectively. (b) The spectral function of the model in the equilibrium excitonic phase with the temperature $T = 116$ K. (c) The sketch for the minimal model. There are three atoms and five orbitals in a unit cell. Orbital 1 on the Ni atom is the lower orbital. Orbitals 2 and 3 on two Ta atoms are upper orbitals, while orbitals 4 and 5 are flat orbitals. They mainly contribute to the corresponding bands, respectively. The orthorhombic-monoclinic structure phase transition will occur as indicated by black arrows at a low temperature.

II. MODEL

In Fig. 1(a), we display the original energy bands obtained from density-functional theory (DFT) calculations, categorized into three classes: lower bands, upper bands, and flat bands. To construct the minimal model, we select five Wannier orbitals from three atoms within a unit cell, as depicted in Fig. 1(c). The Hamiltonian without the external field can be expressed as

$$H_{eq} = \sum_{k,\alpha,\alpha',\sigma} \epsilon_{k,\alpha,\alpha'} c^\dagger_{k,\alpha,\sigma} c_{k,\alpha',\sigma} + H_U + H_V, \quad (1)$$

where the first part is the single-particle Hamiltonian and the others are many-body interactions. Here, we exclusively consider the density-density interactions between orbitals residing on the same atom and on nearest-neighbor Ta-Ni atoms,

$$H_U = \sum_{i,\alpha} U_\alpha n_{i,\alpha,\uparrow} n_{i,\alpha,\downarrow}, \quad (2)$$

$$H_V = \sum_{i,\sigma,\sigma'} [V_{Ta}(n_{i,2,\sigma} n_{i,4,\sigma'} + n_{i,3,\sigma} n_{i,5,\sigma'})$$
$$+ V_{TaNi} n_{i,1,\sigma}(n_{i,2,\sigma'} + n_{i,3,\sigma'} + n_{i,4,\sigma'} + n_{i,5,\sigma'}$$
$$+ n_{i+1,2,\sigma'} + n_{i+1,4,\sigma'} + n_{i-1,3,\sigma'} + n_{i-1,5,\sigma'})], \quad (3)$$

where i denotes the cell's position in the Γ-X direction, α represents the orbital label, and σ represents the spin. A detailed analysis of both the real material and the model is provided in the Supplemental Material [51]. We define the order parameter ϕ by the off-diagonal terms of the density matrix $\rho_{\alpha\alpha'}(x)$ in the real space [46],

$$\phi = \frac{|\rho_{12}(1)| + |\rho_{13}(-1)| - |\rho_{12}(0)| - |\rho_{13}(0)|}{4}. \quad (4)$$

The order parameter measures the asymmetry of the hybridization between the lower orbital of the Ni atom and the upper orbitals of the nearest-neighbor Ta atoms. It is close to zero in the orthorhombic phase and has a nonzero value in the monoclinic phase. In Fig. 1(b), we present the equilibrium spectral function (i.e., the imaginary part of the retarded Green's function G^{ret}) of this model in the ordered phase at a temperature $T = 116$ K. We plot the contributions from different orbitals for the equilibrium spectral function in Fig. 2(a). The band inversion between the upper and lower bands, along with the strong hybridization between the flat and lower bands, is distinctly visible near the Γ point.

To simulate the laser-induced nonequilibrium dynamics, we utilize the nonequilibrium Green's function library NESSi [48], and the length gauge is applied to describe the coupling of light and matter in the Hamiltonian [52–55]. If the position operator is diagonal on the basis of Wannier functions $\langle 0\alpha|r|R\alpha'\rangle = \delta_{0R}\delta_{\alpha\alpha'}\tau_\alpha$, the Hamiltonian in the presence of a laser field can be written as

$$H(k) = H_{eq}(k - A) + \sum_\alpha E\tau_\alpha, \quad (5)$$

where A and E represent the vector potential and electric field of the laser pulse, respectively, τ_α denotes the center position of the orbital α within the unit cell.

III. TIME-DEPENDENCE ANALYSIS

First, we will analyze cases in the time domain. The electric field of the laser pulse we use is given by $E(t) = \sqrt{I}\exp(-t^2/\tau^2)\sin(\omega t)$, with specific parameters $\tau = 4.5$ fs and $\omega = 1.55$ eV and intensity I in arbitrary units. For the case of $I = 0.5$, snapshot of the photoemission spectrum (i.e., the lesser Green's function $G^<$) at $t = 29.6$ fs is plotted in Fig. 2(b). It is evident that some electrons are trapped in the flat band, which has been observed in experiments [56]. To show the situation near the Fermi surface more clearly, Fig. 2(d) shows zoomed-in photoemission spectrum slices at $k = 0$ for various time points of two cases of $I = 0.5$ and 0.2. These two figures reveal that the valence band experiences significant depletion and broadening.

Focusing on the peak's position evolution in Fig. 2(d), we observe that the peak's energy in the case of $I = 0.5$ consistently remains below that of the equilibrium state, while in the case of $I = 0.2$ the peak moves upwards. We will analyze the intensity dependence later and concentrate on the $I = 0.5$ case for now. To identify the underlying cause of the downward shift, we plot the population of the upper and flat orbitals against time in Fig. 2(e). There is a significant transfer from lower orbitals to flat orbitals during the laser pulse, which can be attributed to the resonance between lower bands and flat
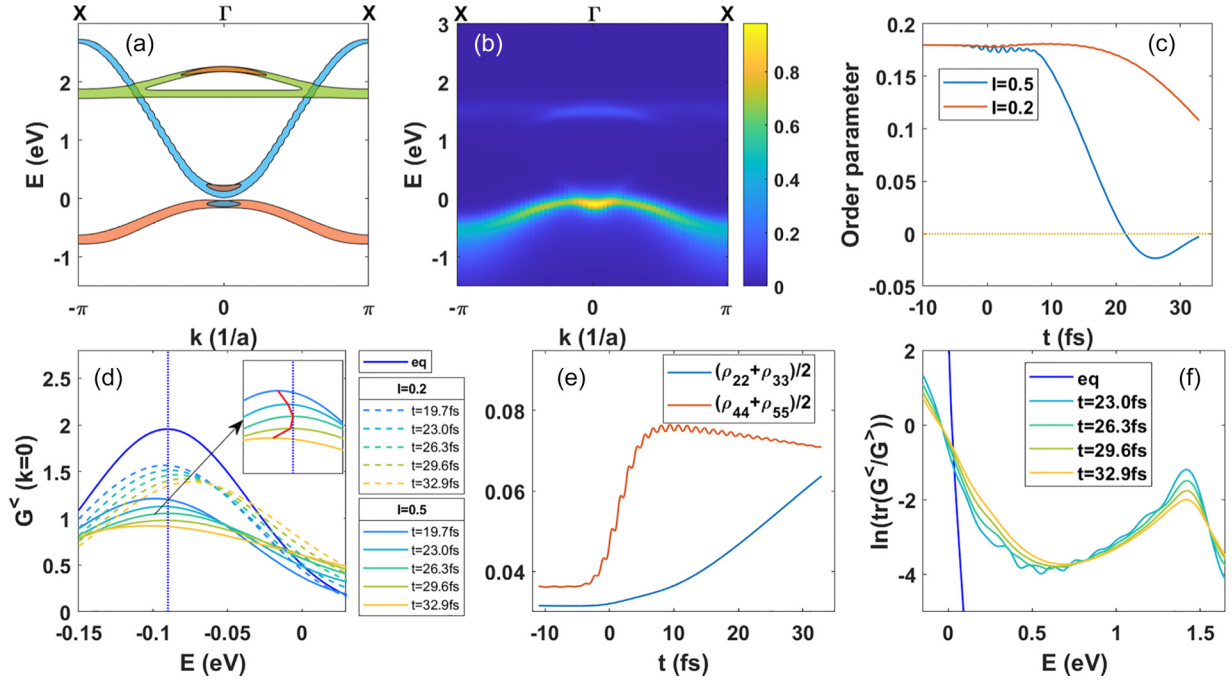
FIG. 2. (a) The contribution of different orbitals to the equilibrium spectral function. Colors are the same as those in Fig. 1. (b) The photoemission spectrum for the case of $I = 0.5$ at $t = 29.6$ fs. (c) The time dependence of the order parameter. (d) The photoemission spectrum at the Γ point for two different cases at different times. "eq" represents the result of the equilibrium state. The red line indicates the shift of the peak for the case of $I = 0.5$. (e) The time dependence of the average local occupation (diagonal terms of the density matrix at $x = 0$) of upper orbitals and flat orbitals for the case of $I = 0.5$. (f) $\ln[\mathrm{tr}(G^</G^>)]$ at different times for the case of $I = 0.5$.

bands near the Γ point and the strong hybridization between the two bands. After the laser pulse, the gradual depletion of flat bands suggests that the trapped state in the flat bands is long-lasting; its lifetime can be estimated as 200 fs by a linear extrapolation. The relaxation process also induces the transfer of population from the lower orbitals to the upper orbitals. Assuming the population transfer from lower orbitals to flat orbitals is Δn_1 and that from lower orbitals to upper orbitals is Δn_2, one can express the Hartree shifts [57] of the bare lower and upper orbitals as

$$\Delta E_{\mathrm{upper}} = \left(\frac{V_{\mathrm{Ta}}}{2} - 2V_{\mathrm{TaNi}}\right)\Delta n_1 + \left(\frac{U_{\mathrm{Ta}}}{4} - 2V_{\mathrm{TaNi}}\right)\Delta n_2,$$

$$\Delta E_{\mathrm{lower}} = \left(2V_{\mathrm{TaNi}} - \frac{U_{\mathrm{Ni}}}{2}\right) \times (\Delta n_1 + \Delta n_2). \tag{6}$$

The coefficients come from the fact that the local interaction exists only between electrons with different spins, and one Ni atom is accompanied by two Ta atoms in a unit cell. According to the parameters from DFT [51], it holds true that $\Delta E_{\mathrm{lower}} > 0$ and $\Delta E_{\mathrm{upper}} < 0$ for any positive values Δn_1 and Δn_2. As TNS is a topological insulator with band inversions [58], its valence top is predominantly contributed by upper orbitals, resulting in a negative Hartree shift $\Delta E_{\mathrm{upper}}$. In addition to the contribution from the Hartree shift, the peak position is also influenced by the order parameter dynamics (the screened Fock term). A photoinduced reduction of the order parameter leads to the collapse of the energy gap (mark the difference with the BEC case [43]) and an upward shift of the valence band. The band shift near the Γ point is sensitive

to the competition of the Hartree shift and the collapse effect. In the case of $I = 0.5$, the Hartree shift prevails. A similar competition has been discussed in other materials [59]. The flat band plays an important role in the balance of two contributions. In Fig. 2(f), the ratio of the lesser Green's function and the greater function $\ln[\mathrm{tr}(G^</G^>)]$ is plotted for different times, and its slope provides an indication of the effective inverse temperature using the fluctuation-dissipation theorem. The symmetry-induced limited hybridization between flat and upper orbitals induces the long-lived states [51] in flat bands and slows down the thermalization and the collapse near the Fermi surface, which makes two contributions comparable. We emphasize that our simulations only cover a brief period immediately following the pulse to illustrate the potential for a downward shift. For longer-term evolution, the effect introduced by phonons becomes significant [60,61], but this is beyond the scope of this study.

IV. LASER-INTENSITY DEPENDENCE ANALYSIS

To examine the anomalous intensity-dependence and momentum-dependence band shifts, we fix the observed time at $t = 29.6$ fs while adjusting the intensity of the pump pulse. The photoemission spectra at $k = 0$ and $k = 1/a$ for a being the lattice distance are illustrated in Figs. 3(a) and 3(b), respectively. A monotonically upward trend in the peak position at $k = 1/a$ is observed with the increase of laser intensity. In contrast, at $k = 0$, the peak position ascends at a lower laser intensity and declines at a higher laser intensity. This observation is consistent with the experimental findings
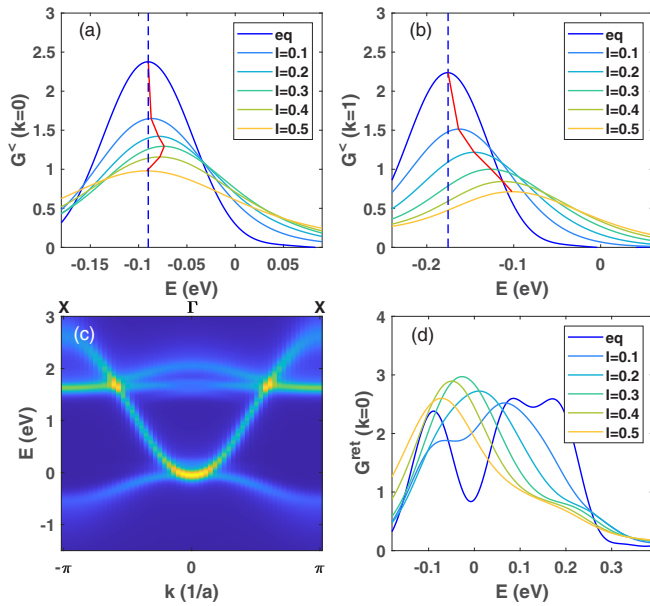
FIG. 3. The photoemission spectrum at $k = 0$ (a) and $k = 1/a$ (b) at $t = 29.6$ fs for different laser intensities I. (c) The spectral function at $t = 29.6$ fs for the laser intensity $I = 0.5$. (d) The spectral function at Γ and $t = 29.6$ fs for different laser intensities.
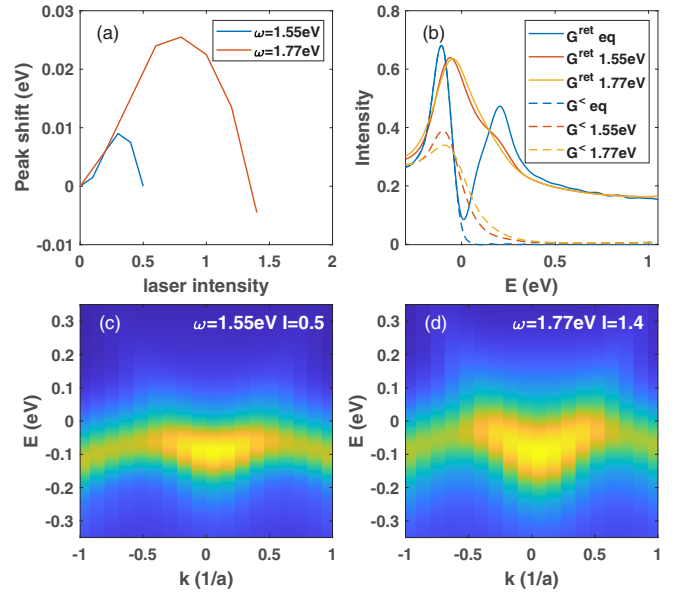

FIG. 4. (a) The laser intensity dependence of the shift of the photoemission spectrum peak at $k = 0$ and $t = 26.3$ fs for two different frequencies. (b) The photoemission spectrum and the spectral function for the equilibrium state, the case of $\omega = 1.55$ eV, $I = 0.5$, and the case of $\omega = 1.77$ eV, $I = 1.4$. (c) The photoemission spectrum near the Γ point at $t = 26.3$ fs for the case of $I = 0.5$, $\omega = 1.55$ eV. (d) Same as (c) but for the case of $I = 1.4$, $\omega = 1.77$ eV.

[17]. The anomalous momentum-dependent band renormalization can be explained by distinct orbital contributions at different momenta. The valence band at $k = 1/a$ is primarily contributed by the lower orbital, so the Hartree shift ΔE_{lower} in Eq. (6) and the collapse effect both lift the band. To elucidate the reason for the anomalous intensity dependence at $k = 0$, we depict the spectral function for $I = 0.5$ in Fig. 3(c), and we provide slices of the spectral function at $k = 0$ for varying laser intensities in Fig. 3(d). With an increase in the intensity of the pump laser, the three peaks observed in the equilibrium spectral function merge, and the energy gap gradually diminishes, illustrating the aforementioned collapse effect. When the intensity is lower than $I = 0.3$, the collapse effect is more pronounced than the Hartree shift, causing the band to move upwards. For higher intensities, although the collapse effect saturates, the Hartree shift does not; it continues to maintain a roughly proportional relationship with the laser intensity [51]. Consequently, it dominates in this scenario, resulting in the downward movement of the band. Numerous experiments also reported the metallization in photoexcited TNS [62–65]. It is hard to define the metallization clearly as a given level of excitations for a transient state. But the downward shift of the valence peak does not contradict the partial metallization induced by the increase in the in-gap spectral function. Our simulations also show the metallization to a certain extent at the same time, as depicted in Figs. 2(b), 3(c), and 3(d). The anomalous intensity-dependent change actually reflects the nonlinear response to the laser field. As the laser intensity increases, the dominated effect may switch due to different nonlinear thresholds. Similar anomalous phenomena have been observed in the absorption peak of other two-dimensional materials with excitonic structures [66,67].

V. LASER-FREQUENCY DEPENDENCE ANALYSIS

Note that not all the experiments report the downward shift of the valence-band top. An example can be found in Ref. [45]. From our data, we can suggest a solution for the discrepancy by the use of a pump laser with a frequency $\omega = 1.77$ eV. As the current minimal model description is a rather rough approximation for the flatband dispersion, future work is needed to confirm the hypothesis. To investigate the effect of frequency, we perform numerical calculations for the laser frequency $\omega = 1.77$ eV to compare with those results with $\omega = 1.55$ eV. The peak shift results for both frequencies are plotted versus the laser intensities in Fig. 4(a). The case with the frequency $\omega = 1.55$ eV exhibits a downward shift behavior at significantly lower intensities. In our opinion, this can be attributed to the proximity of $\omega = 1.55$ eV to the resonant frequency between the lower band and flat bands. A slight detuning leads to a more effective pumping of electrons into the flat bands (larger Hartree shift) with a smaller heating (collapse) effect, and the heating effect will decrease the order parameter and the Fock term, which induces the energy gap of EI. This illustrates that the modulation of the low-energy energy gap can be indirectly influenced by the selective population of high-energy quasiparticles. To investigate the condition under which the downward shift occurs, we select two examples: $\omega = 1.55$ eV with $I = 0.5$ and $\omega = 1.77$ eV with $I = 1.4$. The momentum-integrated spectrum functions and photoemission spectra at 26.3 fs for both examples are shown in Fig. 4(b). Furthermore, the momentum-resolved photoemission spectra at 26.3 fs of two examples are shown in Figs. 4(c) and 4(d). The distortion of the valence band for $\omega = 1.55$ eV is considerably smaller than that in the

high-frequency case, consistent with observations in Refs. [21,45]. Although we still observe a downward shift for $\omega = 1.77$ eV at a higher intensity, the strongly distorted electronic structure under this condition raises concerns about the validity of our model in that condition. The selective excitation exemplified in this paragraph is common in other photodoped materials [7,16,68] and usually indicates a complex excited-state structure, such as the Van Hove singularity.

VI. DISCUSSION

Although we have focused on TNS, this work introduces new and generic strategies for the band-gap renormalization in diverse materials. Here, we gather necessary properties of materials for the anomalous band renormalization. First, a strong Coulomb interaction proves to be pivotal for observing the photoinduced band renormalization. Consequently, low-dimensional materials stand out as promising platforms due to their less screened interaction. Additionally, the existence of long-lived nonequilibrium states is crucial. For the anomalous parameter dependence, the existence of competing mechanisms is a key point. Notably, the band inversion may induce anomalies in momentum dependence, suggesting that topological insulators with band inversions may exhibit similar anomalies in the momentum space. The intensity dependence implies nonlinear responses, while the frequency dependence implies a specific excited-state structure. Past experiments highlight materials with excitonic structures as candidates likely to display an anomalous dependence on the laser parameter in photoinduced phenomena [66,67].

VII. CONCLUSION

We have developed a concise model for TNS and conducted systematic simulations to explore its laser-induced nonequilibrium electronic dynamics. The anomalous parameter dependence of the photoemission spectra is carefully analyzed. This investigation not only sheds light on the anomalous band renormalization in TNS, but it also provides insights for identifying other materials with similar features and designing laser protocols to unveil anomalous photoinduced phenomena. As low-dimensional materials and systems with moire patterns [69–75] generically possess flat bands, we envision these systems as natural candidates for long-lived photomodification of the band structure.

[1] T. Oka and S. Kitamura, Floquet engineering of quantum materials, Annu. Rev. Condens. Matter Phys. **10**, 387 (2019).

[2] A. de la Torre, D. M. Kennes, M. Claassen, S. Gerber, J. W. McIver, and M. A. Sentef, *Colloquium*: Nonthermal pathways to ultrafast control in quantum materials, Rev. Mod. Phys. **93**, 041002 (2021).

[3] H. Aoki, N. Tsuji, M. Eckstein, M. Kollar, T. Oka, and P. Werner, Nonequilibrium dynamical mean-field theory and its applications, Rev. Mod. Phys. **86**, 779 (2014).

[4] Y. Murakami, D. Golež, M. Eckstein, and P. Werner, Photo-induced nonequilibrium states in Mott insulators, arXiv:2310.05201.

[5] A. Disa, J. Curtis, M. Fechner, A. Liu, A. von Hoegen, M. Först, T. Nova, P. Narang, A. Maljuk, A. Boris *et al.*, Photo-induced high-temperature ferromagnetism in $YTiO_3$, Nature (London) **617**, 73 (2023).

[6] R. Mankowsky, A. Subedi, M. Först, S. O. Mariager, M. Chollet, H. Lemke, J. S. Robinson, J. M. Glownia, M. P. Minitti, A. Frano *et al.*, Nonlinear lattice dynamics as a basis for enhanced superconductivity in $YBa_2Cu_3O_{6.5}$, Nature (London) **516**, 71 (2014).

[7] M. Mitrano, A. Cantaluppi, D. Nicoletti, S. Kaiser, A. Perucchi, S. Lupi, P. Di Pietro, D. Pontiroli, M. Riccò, S. R. Clark *et al.*, Possible light-induced superconductivity in K_3C_{60} at high temperature, Nature (London) **530**, 461 (2016).

[8] D. Fausti, R. I. Tobey, N. Dean, S. Kaiser, A. Dienst, M. C. Hoffmann, S. Pyon, T. Takayama, H. Takagi, and A. Cavalleri, Light-induced superconductivity in a stripe-ordered cuprate, Science **331**, 189 (2011).

[9] L. Stojchevska, I. Vaskivskyi, T. Mertelj, P. Kusar, D. Svetin, A. Brazovskii, and D. Mihailovic, Ultrafast switching to a stable hidden quantum state in an electronic crystal, Science **344**, 177 (2014).

[10] I. Vaskivskyi, I. A. Mihailovic, S. Brazovskii, J. Gospodaric, T. Mertelj, D. Svetin, P. Sutar, and D. Mihailovic, Fast electronic resistance switching involving hidden charge density wave states, Nat. Commun. **7**, 11442 (2016).

[11] A. Kogar, A. Zong, P. E. Dolgirev, X. Shen, J. Straquadine, Y.-Q. Bie, X. Wang, T. Rohwer, I.-C. Tung, Y. Yang, R. Li, J. Yang, S. Weathersby, S. Park, M. E. Kozina, E. J. Sie, H. Wen, P. Jarillo-Herrero, I. R. Fisher, X. Wang *et al.*, Light-induced charge density wave in $LaTe_3$, Nat. Phys. **16**, 159 (2020).

[12] A. Zong, P. E. Dolgirev, A. Kogar, E. Ergeçen, M. B. Yilmaz, Y.-Q. Bie, T. Rohwer, I.-C. Tung, J. Straquadine, X. Wang, Y. Yang, X. Shen, R. Li, J. Yang, S. Park, M. C. Hoffmann, B. K. Ofori-Okai, M. E. Kozina, H. Wen, X. Wang *et al.*, Dynamical slowing-down in an ultrafast photoinduced phase transition, Phys. Rev. Lett. **123**, 097601 (2019).

[13] F. Boschini, M. Zonno, and A. Damascelli, Time- and angle-resolved photoemission studies of quantum materials, Rev. Mod. Phys. **96**, 015003 (2024).

[14] L. Perfetti, P. A. Loukakos, M. Lisowski, U. Bovensiepen, H. Berger, S. Biermann, P. S. Cornaglia, A. Georges, and M. Wolf, Time evolution of the electronic structure of $1T$-TaS_2 through the insulator-metal transition, Phys. Rev. Lett. **97**, 067402 (2006).

[15] L. Perfetti, P. A. Loukakos, M. Lisowski, U. Bovensiepen, M. Wolf, H. Berger, S. Biermann, and A. Georges, Femtosecond

dynamics of electronic states in the Mott insulator $1T$-TaS_2 by time resolved photoelectron spectroscopy, New J. Phys. **10**, 053019 (2008).

[16] M. Ligges, I. Avigo, D. Golež, H. U. R. Strand, Y. Beyazit, K. Hanff, F. Diekmann, L. Stojchevska, M. Kalläne, P. Zhou, K. Rossnagel, M. Eckstein, P. Werner, and U. Bovensiepen, Ultrafast doublon dynamics in photoexcited $1T$-TaS_2, Phys. Rev. Lett. **120**, 166401 (2018).

[17] S. Mor, M. Herzog, D. Golež, P. Werner, M. Eckstein, N. Katayama, M. Nohara, H. Takagi, T. Mizokawa, C. Monney *et al.*, Ultrafast electronic band gap control in an excitonic insulator, Phys. Rev. Lett. **119**, 086401 (2017).

[18] S. Zhou, C. Bao, B. Fan, H. Zhou, Q. Gao, H. Zhong, T. Lin, H. Liu, P. Yu, P. Tang *et al.*, Pseudospin-selective Floquet band engineering in black phosphorus, Nature (London) **614**, 75 (2023).

[19] F. Liu, M. E. Ziffer, K. R. Hansen, J. Wang, and X. Zhu, Direct determination of band-gap renormalization in the photoexcited monolayer MoS_2, Phys. Rev. Lett. **122**, 246803 (2019).

[20] D. Wegkamp, M. Herzog, L. Xian, M. Gatti, P. Cudazzo, C. L. McGahan, R. E. Marvel, R. F. Haglund, Jr., A. Rubio, M. Wolf *et al.*, Instantaneous band gap collapse in photoexcited monoclinic VO_2 due to photocarrier doping, Phys. Rev. Lett. **113**, 216401 (2014).

[21] E. Baldini, A. Zong, D. Choi, C. Lee, M. H. Michael, L. Windgaetter, I. I. Mazin, S. Latini, D. Azoury, B. Lv *et al.*, The spontaneous symmetry breaking in Ta_2NiSe_5 is structural in nature, Proc. Natl. Acad. Sci. USA **120**, e2221688120 (2023).

[22] F. Andreatta, H. Rostami, A. Grubišić Čabo, M. Bianchi, C. E. Sanders, D. Biswas, C. Cacho, A. J. H. Jones, R. T. Chapman, E. Springate, P. D. C. King, J. A. Miwa, A. Balatsky, S. Ulstrup, and P. Hofmann, Transient hot electron dynamics in single-layer TaS_2, Phys. Rev. B **99**, 165421 (2019).

[23] M. Puppin, C. W. Nicholson, C. Monney, Y. Deng, R. P. Xian, J. Feldl, S. Dong, A. Dominguez, H. Hübener, A. Rubio, M. Wolf, L. Rettig, and R. Ernstorfer, Excited-state band structure mapping, Phys. Rev. B **105**, 075417 (2022).

[24] N. F. Mott, The transition to the metallic state, Philos. Mag. **6**, 287 (1961).

[25] D. Jérome, T. Rice, and W. Kohn, Excitonic insulator, Phys. Rev. **158**, 462 (1967).

[26] B. Halperin and T. Rice, Possible anomalies at a semimetal-semiconductor transition, Rev. Mod. Phys. **40**, 755 (1968).

[27] J. Eisenstein, Exciton condensation in bilayer quantum Hall systems, Annu. Rev. Condens. Matter Phys. **5**, 159 (2014).

[28] J. Li, T. Taniguchi, K. Watanabe, J. Hone, and C. Dean, Excitonic superfluid phase in double bilayer graphene, Nat. Phys. **13**, 751 (2017).

[29] X. Liu, K. Watanabe, T. Taniguchi, B. I. Halperin, and P. Kim, Quantum Hall drag of exciton condensate in graphene, Nat. Phys. **13**, 746 (2017).

[30] H. Cercellier, C. Monney, F. Clerc, C. Battaglia, L. Despont, M. G. Garnier, H. Beck, P. Aebi, L. Patthey, H. Berger, and L. Forró, Evidence for an excitonic insulator phase in $1T$-$TiSe_2$, Phys. Rev. Lett. **99**, 146403 (2007).

[31] C. Monney, E. F. Schwier, M. G. Garnier, N. Mariotti, C. Didiot, H. Beck, P. Aebi, H. Cercellier, J. Marcus, C. Battaglia, H. Berger, and A. N. Titov, Temperature-dependent

photoemission on $1T$-$TiSe_2$: Interpretation within the exciton condensate phase model, Phys. Rev. B **81**, 155104 (2010).

[32] A. Kogar, M. S. Rak, S. Vig, A. A. Husain, F. Flicker, Y. I. Joe, L. Venema, G. J. MacDougall, T. C. Chiang, E. Fradkin, J. van Wezel, and P. Abbamonte, Signatures of exciton condensation in a transition metal dichalcogenide, Science **358**, 1314 (2017).

[33] Y. Wakisaka, T. Sudayama, K. Takubo, T. Mizokawa, M. Arita, H. Namatame, M. Taniguchi, N. Katayama, M. Nohara, and H. Takagi, Excitonic insulator state in Ta_2NiSe_5 probed by photoemission spectroscopy, Phys. Rev. Lett. **103**, 026402 (2009).

[34] T. Kaneko, T. Toriyama, T. Konishi, and Y. Ohta, Orthorhombic-to-monoclinic phase transition of Ta_2NiSe_5 induced by the bose-einstein condensation of excitons, Phys. Rev. B **87**, 035121 (2013).

[35] K. Sugimoto, S. Nishimoto, T. Kaneko, and Y. Ohta, Strong coupling nature of the excitonic insulator state in Ta_2NiSe_5, Phys. Rev. Lett. **120**, 247602 (2018).

[36] K. Seki, Y. Wakisaka, T. Kaneko, T. Toriyama, T. Konishi, T. Sudayama, N. L. Saini, M. Arita, H. Namatame, M. Taniguchi, N. Katayama, M. Nohara, H. Takagi, T. Mizokawa, and Y. Ohta, Excitonic Bose-Einstein condensation in Ta_2NiSe_5 above room temperature, Phys. Rev. B **90**, 155116 (2014).

[37] Y. F. Lu, H. Kono, T. I. Larkin, A. W. Rost, T. Takayama, A. V. Boris, B. Keimer, and H. Takagi, Zero-gap semiconductor to excitonic insulator transition in Ta_2NiSe_5, Nat. Commun. **8**, 14408 (2017).

[38] K. Kim, H. Kim, J. Kim, C. Kwon, J. S. Kim, and B. J. Kim, Direct observation of excitonic instability in Ta_2NiSe_5, Nat. Commun. **12**, 1969 (2021).

[39] P. A. Volkov, M. Ye, H. Lohani, I. Feldman, A. Kanigel, and G. Blumberg, Critical charge fluctuations and emergent coherence in a strongly correlated excitonic insulator, npj Quantum Mater. **6**, 52 (2021).

[40] M. Ye, P. A. Volkov, H. Lohani, I. Feldman, M. Kim, A. Kanigel, and G. Blumberg, Lattice dynamics of the excitonic insulator $Ta_2Ni(Se_{1-x}S_x)_5$, Phys. Rev. B **104**, 045102 (2021).

[41] M. Guan, D. Chen, Q. Chen, Y. Yao, and S. Meng, Coherent phonon assisted ultrafast order-parameter reversal and hidden metallic state in Ta_2NiSe_5, Phys. Rev. Lett. **131**, 256503 (2023).

[42] Y. Murakami, D. Golež, M. Eckstein, and P. Werner, Photoinduced enhancement of excitonic order, Phys. Rev. Lett. **119**, 247601 (2017).

[43] D. Golež, S. K. Y. Dufresne, M..-J. Kim, F. Boschini, H. Chu, Y. Murakami, G. Levy, A. K. Mills, S. Zhdanovich, M. Isobe, H. Takagi, S. Kaiser, P. Werner, D. J. Jones, A. Georges, A. Damascelli, and A. J. Millis, Unveiling the underlying interactions in Ta_2NiSe_5 from photoinduced lifetime change, Phys. Rev. B **106**, L121106 (2022).

[44] T. Saha, D. Golež, G. De Ninno, J. Mravlje, Y. Murakami, B. Ressel, M. Stupar, and P. R. Ribič, Photoinduced phase transition and associated timescales in the excitonic insulator Ta_2NiSe_5, Phys. Rev. B **103**, 144304 (2021).

[45] T. Tang, H. Wang, S. Duan, Y. Yang, C. Huang, Y. Guo, D. Qian, and W. Zhang, Non-Coulomb strong electron-hole binding in Ta_2NiSe_5 revealed by time-and angle-resolved photoemission spectroscopy, Phys. Rev. B **101**, 235148 (2020).

[46] G. Mazza, M. Rösner, L. Windgätter, S. Latini, H. Hübener, A. J. Millis, A. Rubio, and A. Georges, Nature of symmetry breaking at the excitonic insulator transition: Ta_2NiSe_5, Phys. Rev. Lett. **124**, 197601 (2020).

[47] D. Goležˇ, P. Werner, and M. Eckstein, Photoinduced gap closure in an excitonic insulator, Phys. Rev. B **94**, 035121 (2016).

[48] M. Schüler, D. Goležˇ, Y. Murakami, N. Bittner, A. Herrmann, H. U. Strand, P. Werner, and M. Eckstein, NESSi: The non-equilibrium systems simulation package, Comput. Phys. Commun. **257**, 107484 (2020).

[49] L. V. Keldysh, *Diagram Technique for Nonequilibrium Processes*, Selected Papers of Leonid V Keldysh (World Scientific, 2023), pp. 47—55.

[50] L. P. Kadanoff and G. Baym, *Quantum Statistical Mechanics* (Benjamin, New York, 1962).

[51] See Supplemental Material at http://link.aps.org/supplemental/10.1103/PhysRevB.110.115104 for a detailed description of the model and the parameter dependence of the long-lived states, which includes Refs. [69–75].

[52] D. Goležˇ, M. Eckstein, and P. Werner, Multiband nonequilibrium *GW*+EDMFT formalism for correlated insulators, Phys. Rev. B **100**, 235117 (2019).

[53] L. Yue and M. B. Gaarde, Structure gauges and laser gauges for the semiconductor bloch equations in high-order harmonic generation in solids, Phys. Rev. A **101**, 053411 (2020).

[54] R. E. F. Silva, F. Martín, and M. Ivanov, High harmonic generation in crystals using maximally localized Wannier functions, Phys. Rev. B **100**, 195201 (2019).

[55] J. Li, D. Golez, G. Mazza, A. J. Millis, A. Georges, and M. Eckstein, Electromagnetic coupling in tight-binding models for strongly correlated light and matter, Phys. Rev. B **101**, 205140 (2020).

[56] S. Mor, M. Herzog, C. Monney, and J. Stähler, Ultrafast charge carrier and exciton dynamics in an excitonic insulator probed by time-resolved photoemission spectroscopy, Prog. Surf. Sci. **97**, 100679 (2022).

[57] F. Cilento, G. Manzoni, A. Sterzi, S. Peli, A. Ronchi, A. Crepaldi, F. Boschini, C. Cacho, R. Chapman, E. Springate *et al.*, Dynamics of correlation-frozen antinodal quasiparticles in superconducting cuprates, Sci. Adv. **4**, eaar1998 (2018).

[58] X. Ma, G. Wang, H. Mao, Z. Yuan, T. Yu, R. Liu, Y. Peng, P. Zheng, and Z. Yin, Ta$_2$NiSe$_5$: A candidate topological excitonic insulator with multiple band inversions, Phys. Rev. B **105**, 035138 (2022).

[59] C. D. Spataru, L. X. Benedict, and S. G. Louie, *Ab initio* calculation of band-gap renormalization in highly excited gaas, Phys. Rev. B **69**, 205204 (2004).

[60] S.-Q. Hu, H. Zhao, C. Lian, X.-B. Liu, M.-X. Guan, and S. Meng, Tracking photocarrier-enhanced electron-phonon coupling in nonequilibrium, npj Quantum Mater. **7**, 14 (2022).

[61] S. Mor, M. Herzog, J. Noack, N. Katayama, M. Nohara, H. Takagi, A. Trunschke, T. Mizokawa, C. Monney, and J. Stähler, Inhibition of the photoinduced structural phase transition in the excitonic insulator Ta$_2$NiSe$_5$, Phys. Rev. B **97**, 115154 (2018).

[62] K. Okazaki, Y. Ogawa, T. Suzuki, T. Yamamoto, T. Someya, S. Michimae, M. Watanabe, Y. Lu, M. Nohara, H. Takagi *et al.*, Photo-induced semimetallic states realised in electron–hole coupled insulators, Nat. Commun. **9**, 4322 (2018).

[63] T. Suzuki, Y. Shinohara, Y. Lu, M. Watanabe, J. Xu, K. L. Ishikawa, H. Takagi, M. Nohara, N. Katayama, H. Sawa, M. Fujisawa, T. Kanai, J. Itatani, T. Mizokawa, S. Shin, and K. Okazaki, Detecting electron-phonon coupling during photoinduced phase transition, Phys. Rev. B **103**, L121105 (2021).

[64] T. Miyamoto, M. Mizui, N. Takamura, J. Hirata, H. Yamakawa, T. Morimoto, T. Terashige, N. Kida, A. Nakano, H. Sawa, and H. Okamoto, Charge and lattice dynamics in excitonic insulator Ta$_2$NiSe$_5$ investigated using ultrafast reflection spectroscopy, J. Phys. Soc. Jpn. **91**, 023701 (2022).

[65] K. Katsumi, A. Alekhin, S.-M. Souliou, M. Merz, A.-A. Haghighirad, M. Le Tacon, S. Houver, M. Cazayous, A. Sacuto, and Y. Gallais, Disentangling lattice and electronic instabilities in the excitonic insulator candidate Ta$_2$NiSe$_5$ by nonequilibrium spectroscopy, Phys. Rev. Lett. **130**, 106904 (2023).

[66] T. Jiang, R. Chen, X. Zheng, Z. Xu, and Y. Tang, Photo-induced excitonic structure renormalization and broadband absorption in monolayer tungsten disulphide, Opt. Express **26**, 859 (2018).

[67] S. K. Bera, M. Shrivastava, K. Bramhachari, H. Zhang, A. K. Poonia, D. Mandal, E. M. Miller, M. C. Beard, A. Agarwal, and K. V. Adarsh, Atomlike interaction and optically tunable giant band-gap renormalization in large-area atomically thin MoS$_2$, Phys. Rev. B **104**, L201404 (2021).

[68] S. Pagliara, G. Galimberti, S. Mor, M. Montagnese, G. Ferrini, M. Grandi, P. Galinetto, and F. Parmigiani, Photoinduced π-π^* band gap renormalization in graphite, J. Am. Chem. Soc. **133**, 6318 (2011).

[69] G. Kresse and J. Furthmüller, Efficient iterative schemes for *ab initio* total-energy calculations using a plane-wave basis set, Phys. Rev. B **54**, 11169 (1996).

[70] L. Windgätter, M. Rösner, G. Mazza, H. Hübener, A. Georges, A. J. Millis, S. Latini, and A. Rubio, Common microscopic origin of the phase transitions in Ta$_2$NiSe$_5$ and the excitonic insulator candidate Ta$_2$NiSe$_5$, npj Comput. Mater. **7**, 210 (2021).

[71] A. Subedi, Orthorhombic-to-monoclinic transition in Ta$_2$NiSe$_5$ due to a zone-center optical phonon instability, Phys. Rev. Mater. **4**, 083601 (2020).

[72] A. A. Mostofi, J. R. Yates, Y.-S. Lee, I. Souza, D. Vanderbilt, and N. Marzari, WANNIER90: A tool for obtaining maximally-localised wannier functions, Comput. Phys. Commun. **178**, 685 (2008).

[73] F. Aryasetiawan, M. Imada, A. Georges, G. Kotliar, S. Biermann, and A. I. Lichtenstein, Frequency-dependent local interactions and low-energy effective models from electronic structure calculations, Phys. Rev. B **70**, 195104 (2004).

[74] M. P. von Friesen, C. Verdozzi, and C.-O. Almbladh, Kadanoff-Baym Dynamics of Hubbard clusters: Performance of many-body schemes, correlation-induced damping and multiple steady and quasi-steady states, Phys. Rev. B **82**, 155108 (2010).

[75] M. D. Watson, I. Marković, E. A. Morales, P. Le Fèvre, M. Merz, A. A. Haghighirad, and P. D. C. King, Band hybridization at the semimetal-semiconductor transition of Ta$_2$NiSe$_5$ enabled by mirror-symmetry breaking, Phys. Rev. Res. **2**, 013236 (2020).